A Cryospectroscopic Study of the van der Waals Complexes between Vinyl Fluoride and Boron Trifluoride: Evidence for the Existence of σ and π Complexes

W. A. Herrebout,[†] J. Lundell,[‡] and B. J. van der Veken*[,†]

Department of Chemistry, Universitair Centrum Antwerpen, Groenenborgerlaan 171, B-2020 Antwerp, Belgium, and Laboratory of Physical Chemistry, Department of Chemistry, P.O. Box 55 (A.I. Virtasen aukio 1), FIN-00014 University of Helsinki, Finland

Received: July 16, 1998; In Final Form: September 16, 1998

The complexes formed between vinyl fluoride and BF_3 have been investigated by studying the mid-infrared (4000−400 cm^{-1}) spectra of solutions of the compounds in liquefied argon and in solid argon matrixes. In both types of spectra, evidence was found for 1:1 van der Waals complexes. Ab initio molecular orbital calculations at the MP2/6-31+G(d) level indicate that the complexation can occur via the fluorine atom, giving rise to a σ complex, or via the C═C bond, resulting in a π complex. From a comparison of the experimental and theoretical frequencies, it was concluded that all complex bands observed in the spectra of the cryogenic solutions are due to the σ species. In the spectra of the solid matrixes not only bands of the σ complex, but also weak bands due to the π complex are observed. Using spectra recorded at several temperatures between 97 and 123 K, the complexation enthalpy $\Delta H°$ for the σ complex in LAr was determined to be −11.2(3) kJ mol^{-1}. Using a SCRF/SCIPCM model to correct for the solvent influences and using statistical thermodynamics to account for zero-point vibrational and thermal contributions, the gas-phase complexation energy for this complex was derived to be −15.2(3) kJ mol^{-1}.

Introduction

Boron trifluoride dissolved in liquefied inert gases is known to form van der Waals complexes with various methyl halides[1,2] and with molecules containing π bonds, such as ethene.[3] For the methyl halides, a so-called σ complex is formed between the alkyl halogen atom and the boron atom of BF_3, while with ethene the π electrons act as electron donors in the formation of a π complex. For the complex between methyl fluoride and BF_3 a complexation enthalpy $\Delta H°$ of −16.8 (5) kJ mol^{-1} has been determined in cryosolution,[1] while, for the complex between ethene and BF_3[3] the $\Delta H°$, under similar circumstances, has been derived to be −10.0 (2) kJ mol^{-1}. Thus, at least for isolated halogen atoms or π bonds, the bonding in the π complex is significantly weaker than in the σ complex. In a molecule such as vinyl fluoride, both types of electron donors are present.[4,5] The donor sites are in each others vicinity, which could alter their characteristics. This raises the question as to which types of complexes this compound forms with BF_3 in experiments in which weak complexes are likely to occur. Therefore, using infrared spectroscopy, we have investigated mixtures of vinyl fluoride and boron trifluoride dissolved in liquefied argon and in liquefied nitrogen and deposited in solid argon matrixes. It will be shown in the following paragraphs that for the cryogenic solutions a single 1:1 complex is present, while for the solid matrixes bands due to two distinct complexes can be observed. For the complex observed in LAr, the stoichiometry and the complexation enthalpy have been determined. In addition, the structures of the observed complexes have been derived from a comparison of the experimental vibrational frequencies with ab initio predictions.

* Corresponding author: e-mail, bvdveken@ruca.ua.ac.be.
[†] Department of Chemistry.
[‡] Laboratory of Physical Chemistry.

Experimental Section

The samples of vinyl fluoride and boron trifluoride were purchased from PCR, Inc., and Union Carbide, respectively. In the spectra of vinyl fluoride, no impurities could be detected, while small amounts of SiF_4 were present as an impurity in the BF_3 used. Both gases were used without further purification.

The cryosolution setup consists of a 4 cm copper cell equipped with wedged silicon windows and suspended in a vacuum shroud. The cell is cooled with boiling liquid nitrogen and is connected to a pressure manifold for filling and evacuation. Solutions were prepared by first condensing the monomers in the cooled cell, followed by condensation of the solvent gas. The solvent gases, argon and nitrogen, were provided by L'Air Liquide and have a stated purity of 99.9999%. The matrix-isolated spectra were obtained by slowly condensing vinyl fluoride/BF_3/Ar mixtures onto a CsI window kept at 8 K in a Leybold ROK 10-300 cryostat.

Infrared spectra were recorded on Bruker IFS 113v and IFS 66v spectrometers, using a globar source, a Ge/KBr beamsplitter, and a broad band MCT detector. For each spectrum, 200 interferograms were averaged, Happ Genzel apodized, and Fourier transformed with a zero filling factor of 4 to produce a spectrum with a resolution of 0.5 cm^{-1}.

The ab initio calculations were performed using the Gaussian94 package.[6] For all calculations, electron correlation was accounted for by using second-order Møller−Plesset perturbation theory including explicitly all electrons, while the Berny optimization[7] was used with the tight convergence criteria. A 6-31+G(d) basis set was used throughout as a compromise between accuracy and applicability to larger systems.

The interaction energies of the weak complexes were calculated by subtracting the calculated energies of the monomers from that of the complex in the dimer-centered basis set.

10.1021/jp9830474 CCC: $15.00
Published on Web 11/14/1998

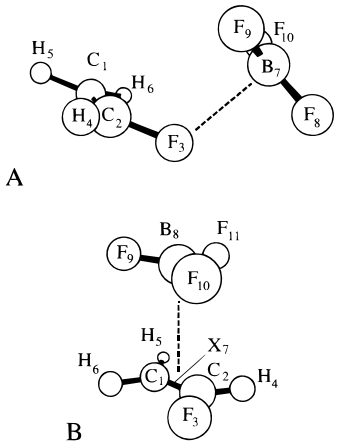

Figure 1. MP2/6-31+G(d) equilibrium geometries for the 1:1 complexes between vinyl fluoride and boron trifluoride: (A) σ complex and (B) π complex.

This corresponds to the counterpoise correction method described by Boys and Bernardi,[8] accounting for the BSSE. For all equilibrium geometries, the vibrational frequencies and the corresponding infrared intensities were calculated with standard harmonic force fields.

The calculations were carried out on the Cray C94 supercomputer at the CSC-Center for Scientific Computing Ltd (Espoo, Finland) and on a Digital Alpha workstation.

Results

1. Ab initio Calculations. To gain insight into the possibilities of complex formation, for both the F···B and the $\pi_{C=C}$···B bonded isomers of the 1:1 complex, further noted as σ-$C_2H_3F{\cdot}BF_3$ and π-$C_2H_3F{\cdot}BF_3$, respectively, structural and spectral information was obtained by carrying out ab initio calculations, at the MP2/6-31+G(d) level. The resulting equilibrium geometries are shown in Figure 1. In addition, the structural parameters of the complexes and those of the monomer molecules are collected in Tables 1 and 2.

From Table 1, it is clear that when forming the σ complex the C−F bond length in vinyl fluoride increases, from 1.3655 to 1.3796 Å. This shows that upon complexation the C−F bond is weakened. Upon complexation, also small changes for the C=C, the C−H, and the B−F bond lengths, varying from −0.002 to +0.004 Å, are predicted. These changes are readily understood from donor−acceptor considerations.[9] The complexation also leads to small deviations from planarity for both the boron trifluoride and the vinyl fluoride moieties.

Upon formation of the π complex, the C=C bond length is calculated to increase from 1.3297 to 1.3321 Å. At the same time, the C−F bond length slightly decreases, from 1.3655 to 1.3611 Å. For both types of complexes, the B−F bond lengths are slightly larger than in the monomer. The average B−F bond length for the π complex, 1.3297 Å, however, is somewhat smaller than the average value of 1.3305 Å obtained for the σ complex. This suggests that the π complex is the weaker one, which is confirmed by the MP2/6-31+G(d) complexation energies. These values are also given in Tables 1 and 2 and, for instance, the uncorrected values decrease from −21.43 kJ mol^{-1} for the σ complex to −14.61 kJ mol^{-1} for the π complex.

In Table 2, the structure of the π complex is described with reference to a dummy atom X_7, which is located at the C=C bond, at the perpendicular projection of the boron atom. The intermolecular distance of the π complex, defined as the distance between B_8 and X_7, was calculated to be 2.951 Å. This value is slightly larger than the similar distance in $C_2H_4{\cdot}BF_3$, 2.922 Å.[3] Also, the average B−F bond length for the present π complex, 1.3297 Å, is slightly smaller than the corresponding quantity obtained for $C_2H_4{\cdot}BF_3$, 1.3303 Å.[3] These results suggest that the present π complex is somewhat weaker than $C_2H_4{\cdot}BF_3$. The complexation energies for π-$C_2H_3F{\cdot}BF_3$ before and after the correction for BSSE, −14.6 kJ mol^{-1} and −4.8 kJ mol^{-1}, indeed are somewhat smaller than the values of −17.3 and −7.4 kJ mol^{-1} obtained for ethene·BF_3.[3] The small destabilization for the vinyl fluoride complex can be explained by the electron-withdrawing effect of the nearby fluorine atom.

TABLE 1: MP2/6-31+G(d) Structural Parameters[a] for σ-$C_2H_3F{\cdot}BF_3$, for C_2H_3F, and for BF_3

	σ-$C_2H_3F{\cdot}BF_3$	C_2H_3F	BF_3
$r(C_1{=}C_2)$	1.3278	1.3297	
$r(C_2{-}F_3)$	1.3796	1.3655	
$r(C_2{-}H_4)$	1.0827	1.0839	
$r(C_1{-}H_5)$	1.0829	1.0826	
$r(C_1{-}H_6)$	1.0832	1.0834	
$r(F_3{\cdots}B_7)$	2.4003		
$r(B_7{-}F_8)$	1.3282		1.3278
$r(B_7{-}F_9)$	1.3317		1.3278
$r(B_7{-}F_{10})$	1.3316		1.3278
$<(F_3{-}C_2{=}C_1)$	120.571	121.477	
$<(H_4{-}C_2{=}C_1)$	128.314	126.977	
$<(H_5{-}C_1{-}C_2)$	118.946	119.137	
$<(H_6{-}C_1{=}C_2)$	121.608	121.543	
$<(B_7{\cdots}F_3{-}C_2)$	118.182		
$<(F_8{-}B_7{\cdots}F_3)$	91.808		
$<(F_9{-}B_7{\cdots}F_3)$	91.929		
$<(F_{10}{-}B_7{\cdots}F_3)$	91.779		
$\tau(H_4{-}C_2{=}C_1{-}F_3)$	179.89	180.00	
$\tau(H_5{-}C_1{=}C_2{-}F_3)$	180.19	180.00	
$\tau(H_6{-}C_1{=}C_2{-}F_3)$	−0.37	0.00	
$\tau(B_7{\cdots}F_3{-}C_2{=}C_1)$	74.74		
$\tau(F_8{-}B_7{\cdots}F_3{-}C_2)$	176.43		
$\tau(F_9{-}B_7{\cdots}F_3{-}F_8)$	120.17		
$\tau(F_{10}{-}B_7{\cdots}F_3{-}F_8)$	−120.20		
dipole moment/debye	2.34	1.67	0.00
energy/hartree	−501.134224	−177.321913	-323.804151
ΔE/kJ mol^{-1}	−21.43		
E_{BSSE}/kJ mol^{-1}	−11.38		
ΔE_{corr}/kJ mol^{-1}	−10.05		

[a] Bond Lengths in angstroms, bond angles in degrees.

TABLE 2: MP2/6-31+G(d) Structural Parameters[a] for π-$C_2H_3F{\cdot}BF_3$

$r(C_1{=}C_2)$	1.3321	$<(X_7{-}C_2{-}F_3)$	121.422
$r(C_2{-}F_3)$	1.3611	$<(B_8{\cdots}X_7{-}C_2)$	90.000
$r(C_2{-}H_4)$	1.0846	$<(F_9{-}B_8{\cdots}X_7)$	90.935
$r(C_1{-}H_5)$	1.0832	$<(F_{10}{-}B_8{\cdots}X_7)$	95.357
$r(C_1{-}H_6)$	1.0839	$<(F_{11}{-}B_8{\cdots}X_7)$	87.546
$r(C_2{-}X_7)$	1.0839		
$r(X_7{\cdots}B_8)$	2.9510	$\tau(H_4{-}C_2{=}C_1{-}F_3)$	180.253
$r(B_8{-}F_9)$	1.3295	$\tau(H_5{-}C_1{=}C_2{-}F_3)$	181.057
$r(B_8{-}F_{10})$	1.3279	$\tau(H_6{-}C_1{=}C_2{-}F_3)$	−0.890
$r(B_8{-}F_{11})$	1.3317	$\tau(X_7{-}C_2{-}F_3{-}C_1)$	0.00
		$\tau(B_8{\cdots}X_7{-}C_2{-}F_3)$	98.02
$<(F_3{-}C_2{=}C_1)$	121.422	$\tau(F_9{-}B_8{\cdots}X_7{-}C_2)$	−153.27
$<(H_4{-}C_2{=}C_1)$	126.784	$\tau(F_{10}{-}B_8{\cdots}X_7{-}F_9)$	120.46
$<(H_5{-}C_1{=}C_2)$	119.049	$\tau(F_{11}{-}B_8{\cdots}X_7{-}F_9)$	−119.76
$<(H_6{-}C_1{=}C_2)$	121.535		
dipole moment/debye		1.55	
energy/hartree		−501.131629	
ΔE/kJ mol^{-1}		−14.61	
E_{BSSE}/kJ mol^{-1}		−9.81	
ΔE_{corr}/kJ mol^{-1}		−4.80	

[a] Bond Lengths in angstroms, bond angles in degrees. X_7 is a dummy atom in the C=C bond, at the perpendicular projection of the B atom.

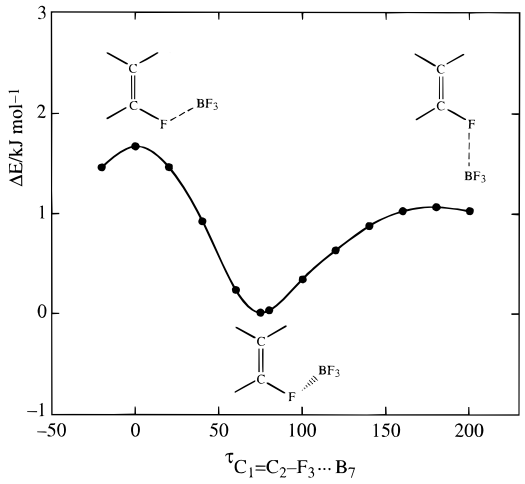

Figure 2. Potential energy function for the internal rotation around the C_2-F_3 bond in σ-$C_2H_3F\cdot BF_3$.

Inherent to the weakness of the van der Waals bonds is the flexibility of the complexes. For the σ complex, this is demonstrated by the barrier hindering internal rotation around (i) the $F_3\cdots B_7$ van der Waals bond and (ii) the C_2-F_3 bond. These barriers were obtained by systematically varying the required angular parameter, and at each value calculating the energy of the complex while relaxing all other structural parameters.

The barrier for (i) was found to be 1.1 kJ mol^{-1}. This value is very low, but is significantly larger than the values of 0.2 and 0.3 kJ mol^{-1} obtained for the BF_3 complexes with ethene[3] and with carbonyl fluoride.[10] The value also is slightly larger than the barrier of 0.7 kJ mol^{-1} obtained for the $CH_3F\cdot BF_3$ complex.[1]

In Figure 2, the potential obtained for the internal rotation (ii), i.e., around the C_2-F_3 bond, is shown. Two separate maxima are present in this potential: a first one with $\tau_{C_1=C_2-F_3\cdots B_7}$ equal to 0° and another at $\tau_{C_1=C_2-F_3\cdots B_7}$ equal to 180°. It can be seen that for (ii) the energy difference between the transition states and the equilibrium geometry is less than 1.5 kJ mol^{-1}. These low barriers suggest that, even at the relatively low temperatures used for the cryosolutions, the σ complex formed between vinyl fluoride and BF_3 will be characterized by large amplitude torsional motions.

The vibrational frequencies and infrared intensities obtained for the complexes and for the constituent molecules are given in Tables 3 and 4. Also given are the complexation shifts $\Delta\nu$, defined as $\nu_{complex} - \nu_{monomer}$. These data will be used to identify the complex species observed below.

Because of the very weak interaction between the monomers, the vibrations of the complexes can be classified as modes localized in the monomers and as intermolecular modes. The intermolecular modes are predicted to occur in the far-infrared. This region was not investigated and thus only modes localized in the constituent molecules can be used for the assignments of the various complexes. These modes can unambiguously be correlated with those of the isolated monomers. Therefore, we will describe such complex modes starting from the assignments of the corresponding monomer modes. For the latter, the standard numbering scheme is used,[11] and the symbol is expanded with the formula of the monomer as a superscript.

Experience with other complexes learns that ab initio calculations tend to predict the correct sign of complexation shifts but that absolute values are often overestimated. Therefore, predicted complexation shifts are of diagnostic value if the shifts for σ and π complexes (i) are sufficiently large and (ii) occur in opposite direction. Inspection of Tables 3 and 4 then shows that only the ν_2, ν_7, ν_8, and ν_{10} modes of C_2H_3F can be used to identify the observed complex. It may be noted that, although the C═C bond length is calculated to slightly decrease in the π complex, its stretching frequency $\nu_4^{C_2H_3F}$ occurs somewhat red shifted. This, most probably, is due to differences in the coupling with $\nu_5^{C_2H_3F}$ in the complex and in the monomer.

When forming a σ complex, the BF_3 asymmetric stretches $\nu_3^{BF_3}$ in the ^{10}B isotopomer are calculated to red shift by 1.9 and 16.7 cm^{-1}, respectively. These shifts compare favorably with those predicted for $CH_3F\cdot BF_3$.[1] In contrast, for the ^{11}B isotopomer one of the BF_3 symmetric stretches is calculated to red shift by ca. 17.8 cm^{-1}, while for the other a small blue shift of approximately 1.1 cm^{-1} is predicted. This, most probably, is a consequence of coupling with $\nu_9^{C_2H_3F}$. Changing the ^{10}B for the ^{11}B isotopomer, both the infrared intensities of the BF_3 asymmetric stretches and the C═C−H in plane deformation indeed strongly change, indicating a strong intensity borrowing from the BF_3 modes toward $\nu_9^{C_2H_3F}$.

2. Vibrational Spectra

The vibrational spectra of monomeric BF_3 and vinyl fluoride in cryosolutions and in solid matrixes have been discussed in detail before,[5,11] and need not be commented upon here. It is well known that the band maxima in cryosolutions shift significantly with temperature.[12,13] Therefore, the frequencies discussed below were taken from spectra recorded at 100.4(4) K.

A. Liquid Argon. Compared with the spectra of the monomers, in the spectra of vinyl fluoride/BF_3 mixtures a large number of new bands are observed. This signals that a complex between vinyl fluoride and BF_3 is being formed. The observed frequencies, their assignments and the complexation shifts are summarized in Table 5. Some of the more important new bands deserve a detailed discussion.

In Figure 3, the 1500−1400 cm^{-1} region of a solution containing 1.5×10^{-4} M BF_3 and 5.0×10^{-3} M vinyl fluoride is compared with that of solutions of the monomers. On the low-frequency side of the $\nu_3^{BF_3}$ bands at 1495.1 and 1444.0 cm^{-1}, for the mixture new bands due to a complex are observed, at 1491.3 and 1482.7 cm^{-1} and at 1440.4 and 1431.8 cm^{-1}. In view of the concentration study to be discussed below, and in view of the ab initio calculations described above, these bands are assigned as the BF_3 antisymmetric stretches of a 1:1 complex of vinyl fluoride with $^{10}BF_3$, and with $^{11}BF_3$, respectively.

The $\nu_2^{BF_3}$ region of a solution containing approximately 0.4×10^{-3} M BF_3 and 5.0×10^{-3} M vinyl fluoride, recorded at several temperatures between 84 and 98 K, is compared with the monomer spectra in Figure 4. In the spectra of the mixtures, new bands can be observed at 675.9 and 650.9 cm^{-1}. These bands are assigned to the $\nu_2^{BF_3}$ modes in the complex with $^{10}BF_3$ and $^{11}BF_3$, respectively.

In the spectra shown in Figure 4, at the lowest temperatures a weak feature emerges at 637 cm^{-1}. Inspection of the spectra suggests that this band must be associated with the ^{11}B isotope, and it is tempting to assign it to the π complex. However, the ab initio calculations predict the $\nu_2^{BF_3}$ mode in the π complex to appear within 0.1 cm^{-1} from the corresponding mode in the σ complex, while the 637 cm^{-1} is red shifted by more than 13 cm^{-1} from its σ counterpart. A band similar to the one at 637 cm^{-1} has been observed for other BF_3 complexes and was

TABLE 3: MP2/6-31+G(d) Vibrational Frequencies (cm^{-1}) and Infrared Intensities (km mol^{-1}) for σ-$C_2H_3F{\cdot}BF_3$, for C_2H_3F, and for BF_3

symmetry, mode numbering, and approximate description			σ-$C_2H_3F{\cdot}^{11}BF_3$			σ-$C_2H_3F{\cdot}^{10}BF_3$			C_2H_3F		$^{11}BF_3$		$^{10}BF_3$	
			ν	intensity	$\Delta\bar{\nu}$	ν	intensity	$\Delta\bar{\nu}$	$\bar{\nu}$	intensity	$\bar{\nu}$	intensity	$\bar{\nu}$	intensity
C_2H_3F submolecule														
A′	$\nu_1^{C_2H_3F}$	CH_2 antisymmetric stretch	3347.7	0.2	1.8	3347.7	0.2	1.8	3345.9	0.7				
	$\nu_2^{C_2H_3F}$	CH stretch	3307.3	2.6	16.6	3307.3	2.6	16.6	3290.7	5.3				
	$\nu_3^{C_2H_3F}$	CH_2 symmetric stretch	3241.4	2.5	1.2	3241.4	2.5	1.2	3240.2	1.2				
	$\nu_4^{C_2H_3F}$	C═C stretch	1719.8	86.7	−3.6	1719.8	87.7	−3.6	1723.4	95.5				
	$\nu_5^{C_2H_3F}$	CH_2 deformation	1437.0	212.2	−8.5	1438.6	12.3	−6.9	1445.5	6.2				
	$\nu_6^{C_2H_3F}$	C═C−H in plane deformation	1349.9	0.5	−4.7	1349.9	0.5	4.7	1354.6	0.5				
	$\nu_7^{C_2H_3F}$	C−F stretch	1150.7	91.3	−21.4	1150.8	90.5	−21.3	1172.1	100.0				
	$\nu_8^{C_2H_3F}$	CH_2 rocking	927.5	49.5	−14.7	927.7	48.0	−14.5	942.2	47.5				
	$\nu_9^{C_2H_3F}$	C═C−F in-plane deformation	481.7	7.1	−1.1	481.8	7.7	−1.0	482.8	4.2				
A″	$\nu_{10}^{C_2H_3F}$	C═C−H out-of-plane deformation	950.7	61.4	−7.1	950.7	61.6	−7.1	957.8	55.6				
	$\nu_{11}^{C_2H_3F}$	CH_2 wagging	886.6	41.7	25.5	886.7	41.8	25.6	861.1	54.9				
	$\nu_{12}^{C_2H_3F}$	CH_2 twist	724.5	4.9	−0.9	724.5	5.8	−0.9	725.4	3.6				
BF_3 submolecule														
A_1'	$\nu_1^{BF_3}$	BF_3 symmetric stretch	865.0	3.5	−7.4	865.0	4.1	−7.4			872.4		872.4	
A_2''	$\nu_2^{BF_3}$	BF_3 out-of-plane bend	652.8	218.2	−42.8	678.4	237.3	−45.7			695.6	118.0	724.1	127.8
E′	$\nu_3^{BF_3}$	BF_3 asymmetric stretch	1443.7	258.6	1.1	1493.7	480.6	−1.9			1442.6	483.1	1495.6	524.0
			1424.8	386.6	−17.8	1478.9	434.6	−16.7						
E′	$\nu_4^{BF_3}$	BF_3 in-plane bend	472.9	12.4	0.9	474.8	12.3	1.0			472.0	15.1	473.8	14.8
			472.4	8.9	0.2	474.2	7.8	0.4						
low-energy deformation modes														
			146.0	8.5		146.2	8.5							
			127.5	0.6		127.6	0.6							
			105.1	3.9		105.3	3.8							
			65.2	2.2		65.2	2.2							
			45.9	0.3		45.9	0.3							
			26.9	1.1		26.8	1.1							

[a] Symmetry species and mode numbers refer to the respective monomer species.

assigned to a complex with higher stoichiometry.[3,12,14] The behavior with concentration and temperature if the intensity of the 637 cm^{-1} band is not incompatible with a similar interpretation, and, therefore, we prefer to assign this band to a complex involving one BF_3 and two vinyl fluoride molecules. This type of complex should also give well separated bands in the $\nu_3^{BF_3}$ region. However, even when a large excess of vinyl fluoride was used, no such bands were observed. The reason for this is not yet understood.

The C−F stretching region of a mixed solution is compared to that of vinyl fluoride in Figure 5. For the mixed solution, a strong complex band is observed at 1132.5 cm^{-1}, i.e., at a frequency 16.4 cm^{-1} lower than that of monomer C_2H_3F. Comparison with the ab initio predictions shows that this band must be assigned to the σ complex. Even at the highest monomer concentrations no complex bands were detected on the high frequency side of the monomer band. Hence, at all times during our experiments the concentration of the π complex was below the detection limit. Using the fact that the ab initio calculations predict $\nu_7^{C_2H_3F}$ to have similar intensities in σ and π complex, from the signal-to-noise ratio in Figure 5 may be concluded that the concentration of the π complex was less than 1% of that of the σ complex. Finally, Figure 5 shows that for the mixed solution a very weak band band is present at 1112.5 cm^{-1}. This band is the complex band corresponding to the weak monomer transition at 1129.0 cm^{-1},[5] and, therefore, is assigned to $\nu_7^{C_2H_3F}$ in σ-$CH_2{}^{13}CHF{\cdot}BF_3$.

In Figure 6, the 960−840 cm^{-1} region of a mixed solution is compared with that of a vinyl fluoride solution. In the spectra of the mixed solutions, weak bands appear at 870.9 and 878.0 cm^{-1} on the high-frequency side of the CH_2 wagging mode $\nu_{11}^{C_2H_3F}$ at 861.6 cm^{-1}. In agreement with the ab initio predictions, these bands are assigned to the CH_2 wagging and the BF_3 symmetric stretching in the 1:1 complex. The latter mode is forbidden in monomer BF_3, but, as in other BF_3 complexes,[1,3,10,12] has induced intensity in the complex.

At the lowest temperatures, a shoulder at 929 cm^{-1} becomes visible on the 925 cm^{-1} monomer band. These bands are assigned to $\nu_{10}^{C_2H_3F}$ (929 cm^{-1}) and $\nu_8^{C_2H_3F}$ (925 cm^{-1}).[5,11] In the spectra of the mixed solution a complex band grows in at 914 cm^{-1}, i.e., red shifted from both monomer bands. This is in agreement with predictions for the σ complex, but contradicts the ab initio results for the π complex. Thus, the 914 cm^{-1} band supports the identification of the complex made above. If we assume that, as for $\nu_7^{C_2H_3F}$, the ab initio calculations overestimate the complexation shifts, the 914 cm^{-1} band must be assigned as $\nu_8^{C_2H_3F}$. For the same reason, it is concluded that the $\nu_{10}^{C_2H_3F}$ complex band appears accidentally degenerate with the 925 cm^{-1} band.

It was observed above that also for $\nu_2^{C_2H_3F}$ a considerable complexation shift is expected. In the experimental spectra of mixed solutions in this region indeed a new band, to be assigned to $\nu_2^{C_2H_3F}$, is observed, blue shifted by +9.2 cm^{-1}. This shift,

TABLE 4: MP2/6-31+G(d) Vibrational Frequencies (cm^{-1}) and Infrared Intensities (km mol^{-1}) for π-$C_2H_3F{\cdot}BF_3$

symmetry, mode numbering, and approximate description[a]			π-$C_2H_3F{\cdot}^{11}BF_3$			π-$C_2H_3F{\cdot}^{10}BF_3$		
			$\bar{\nu}$	intensity	$\Delta\bar{\nu}$	$\bar{\nu}$	intensity	$\Delta\bar{\nu}$
C_2H_3F submolecule								
A′	$\nu_1^{C_2H_3F}$	CH_2 antisymmetric stretch	3343.6	0.0	−2.3	3343.6	0.0	−2.3
	$\nu_2^{C_2H_3F}$	CH stretch	3287.2	3.2	−3.5	3287.2	3.3	−3.5
	$\nu_3^{C_2H_3F}$	CH_2 symmetric stretch	3236.6	3.1	−3.6	3236.6	3.1	−3.6
	$\nu_4^{C_2H_3F}$	C═C stretch	1716.5	101.0	−6.9	1716.6	103.3	−6.9
	$\nu_5^{C_2H_3F}$	CH_2 deformation	1353.2	0.9	−1.4	1353.3	0.7	−1.3
	$\nu_6^{C_2H_3F}$	C═C−H in plane deformation	1446.2	58.8	0.7	1444.9	0.9	−0.6
	$\nu_7^{C_2H_3F}$	C−F stretch	1177.4	81.8	5.3	1177.4	83.0	5.3
	$\nu_8^{C_2H_3F}$	CH_2 rocking	948.0	39.6	5.8	948.1	39.6	5.9
	$\nu_9^{C_2H_3F}$	C═C−F in plane deformation	485.0	4.2	2.2	485.0	4.1	2.2
A″	$\nu_{10}^{C_2H_3F}$	C═C−H out of plane deformation	976.8	51.9	19.0	976.8	61.4	19.0
	$\nu_{11}^{C_2H_3F}$	CH_2 wagging	895.4	50.5	34.3	895.5	47.8	34.4
	$\nu_{12}^{C_2H_3F}$	CH_2 twist	749.6	1.2	24.2	749.7	0.8	24.3
BF_3 submolecule								
A_1'	$\nu_1^{BF_3}$	BF_3 symmetric stretch	865.2	4.6	−7.2	865.2	4.9	−7.2
A_2''	$\nu_2^{BF_3}$	BF_3 out of plane bend	652.7	246.5	−42.9	678.5	269.3	−45.6
E′	$\nu_3^{BF_3}$	BF_3 asymmetric stretch	1439.1	355.3	−3.5	1492.3	411.8	−3.3
			2427.4	11.1	−15.2	1480.8	452.6	−14.8
E′	$\nu_4^{BF_3}$	BF_3 in plane deformation	470.9	11.0	−1.1	472.8	10.7	−1.0
			470.0	11.1	−2.0	471.9	10.8	−1.9
low-energy deformation modes								
			134.3	3.8		134.4	3.8	
			103.6	0.3		103.6	0.3	
			87.1	0.5		87.1	0.5	
			80.7	0.8		80.7	0.8	
			54.5	1.9		54.6	1.9	
			15.9	1.1		15.9	1.1	

[a] Symmetry species and mode numbers refer to the respective monomer species.

again, supports the identification of the complex as σ-$C_2H_3F{\cdot}BF_3$.

Close scrutiny of the overtone regions of the spectra of the mixed solutions reveals the presence of several bands that must be assigned to the complex species. This is illustrated in Figure 7, where the 2600−2000 cm^{-1} region of the spectra is shown. On the low-frequency side of the bands at 2375.2 and 2325.1 cm^{-1} assigned to the $\nu_1^{BF_3} + \nu_3^{BF_3}$ combination in $^{10}BF_3$ and $^{11}BF_3$, new bands due to the corresponding modes in the complex appear near 2310 and 2360 cm^{-1}, respectively. In addition, also for $2\nu_1^{BF_3} + \nu_4^{BF_3}$ at 2235.0 cm^{-1}, a slightly red shifted complex band is observed.

For the first overtone of the C−F stretching, at 2290 cm^{-1} in the monomer, a complex band may be expected, which is shifted from the monomer by an amount twice the complexation shift of the fundamental, i.e., at approximately 2290.9 − [(2)(16.5)] = 2257.9 cm^{-1}. In the spectra of the mixed solutions, such a band is indeed observed at 2257.0 cm^{-1}. The other complex bands in this region were identified using similar arguments. The observed frequencies and their assignments have been collected in Table 5.

On top of new bands assignable to a 1:1 complex, in the spectra shown in Figure 7, weak absorptions due to a second type of complex are observed at 2043.9 and at 2265.5 cm^{-1}. These bands show the same temperature and concentration dependence of their intensity as the 637 cm^{-1} band and, consequently, are also assigned to the 1:2 complex $(C_2H_3F)_2{\cdot}BF_3$.

To complete the analysis of the $C_2H_3F{\cdot}BF_3$ complex, the spectra of mixtures dissolved in liquefied nitrogen have been investigated. Also for these solutions, the formation of a 1:1 complex was concluded from the appearance of new bands close to the BF_3 or the C_2H_3F monomer bands. Because of the similarity with the argon solutions, no detailed description of these bands will be given. It was observed that, when equal concentrations of C_2H_3F and BF_3 are used, the intensities of complex bands observed in LN_2 solutions are much weaker than those observed in LAr. This, as was recently shown,[14] is caused by the fact that in LN_2 the BF_3 molecules form 1:1 and 1:2 complexes with N_2.

B. Argon Matrixes. While solutions in liquid argon are in thermodynamic equilibrium, it is well-known that in solid matrixes less stable adducts can be trapped in addition to the thermodynamically favored products. Therefore, the spectra of various C_2H_3F/BF_3 mixtures deposited in solid argon were also investigated. In Table 6, the complex bands observed for the matrixes, and those observed for the cryogenic solutions are compared.

In Figure 8, the spectrum of a typical $C_2H_3F/BF_3/Ar$ matrix and that of a C_2H_3F/Ar matrix are compared. For the C_2H_3F/Ar matrix absorption bands due to the $\nu_7^{C_2H_3F}$, $\nu_8^{C_2H_3F}$, $\nu_{10}^{C_2H_3F}$, and $\nu_{11}^{C_2H_3F}$ are seen. It may be remarked that in these spectra the bands due to $\nu_8^{C_2H_3F}$ and $\nu_{10}^{C_2H_3F}$ are much better separated than in the solution spectra of Figure 6. In the spectra of the $C_2H_3F/BF_3/Ar$ matrix strong bands due to a complex can be observed at 1126.7, 911.6, and 872.9 cm^{-1}. The frequencies of these bands are similar to those observed in the spectra of the cryogenic solutions and, consequently, must all be assigned to the σ complex. In addition, weak bands are observed at 1153.3 and 957.5 cm^{-1}. The latter occur at frequencies close to those predicted for the π complex. The appearance of these bands, therefore, is taken as evidence that a small fraction of the π complex is trapped in the solid matrixes.

TABLE 5: Vibrational Frequencies (cm^{-1}) Observed in Liquefied Argon (100 K) for BF_3, C_2H_3F, and $C_2H_3F \cdot BF_3$

BF_3 submolecule	$^{11}BF_3$ ($\bar{\nu}$)	$C_2H_3F \cdot {}^{11}BF_3$ $\bar{\nu}$	$\Delta\bar{\nu}$	$^{10}BF_3$ ($\bar{\nu}$)	$C_2H_3F \cdot {}^{10}BF_3$ $\bar{\nu}$	$\Delta\bar{\nu}$
$2\nu_3^{BF_3}$	2885.9	2875.2	−10.7	2989.0	2976.7	−12.3
$\nu_1^{BF_3} + \nu_3^{BF_3} + \nu_4^{BF_3}$	2799.0			2849.4	2838.8	−10.6
$\nu_1^{BF_3} + \nu_3^{BF_3}$	2325.1	2314.6	−10.5	2375.2	2364.4	−10.8
		2306.0	−19.1		2355.8	−19.4
$2\nu_1^{BF_3} + \nu_4^{BF_3}$	2235.0	2223.6	−11.4	2235.0	2223.6	−11.4
$\nu_3^{BF_3}$	1444.0	1440.4	−3.6	1495.1	1491.3	−3.8
		1431.8	−12.2		1482.7	12.4
$\nu_1^{BF_3} + \nu_4^{BF_3}$	1358.0	1351.6	−6.4	1358.0	1351.6	−6.4
$\nu_1^{BF_3}$		*a*	878.0		*a*	878.0
$\nu_2^{BF_3}$	679.8	650.9	−28.9	707.2	675.9	−31.3
$\nu_4^{BF_3}$	474.0			474.0		

vinyl fluoride submolecule	C_2H_3F ($\bar{\nu}$)	$C_2H_3F \cdot BF_3$ $\bar{\nu}$	$\Delta\bar{\nu}$
$\nu_2^{C_2H_3F}$	3103.5	3112.7	+9.2
$\nu_6^{C_2H_3F} + \nu_{10}^{C_2H_3F} + \nu_{11}^{C_2H_3F}$	3093.3	3103.5	+10.2
$\nu_4^{C_2H_3F} + \nu_6^{C_2H_3F}$	2795.0	2776.8	−18.2
$2\nu_5^{C_2H_3F}$	2745.0	2738.1	−6.9
$\nu_4^{C_2H_3F} + \nu_8^{C_2H_3F}$	2569.3	2558.2	−11.1
$\nu_5^{C_2H_3F} + \nu_7^{C_2H_3F}$	2520.4	2500.0	−20.4
$\nu_6^{C_2H_3F} + \nu_7^{C_2H_3F}$	2449.7	2433.2	−16.5
$2\nu_7^{C_2H_3F}$	2290.9	2257.0	−33.9
$\nu_7^{C_2H_3F} + \nu_8^{C_2H_3F}$	2067.5	2039.6	−27.8
$\nu_7^{C_2H_3F} + \nu_{12}^{C_2H_3F}$	1858.2	1839.4	−18.8
$2\nu_8^{C_2H_3F}$	1851.0	1826.6	−24.2
$2\nu_{11}^{C_2H_3F}$	1730.5	1747.0	−16.5
$\nu_{11}^{C_2H_3F} + \nu_{12}^{C_2H_3F}$	1571.4	1577.4	+6.0
$\nu_5^{C_2H_3F}$	1375.7	1372.1	−3.6
$\nu_7^{^{13}C_2H_3F}$	1129.0	1112.5	−16.5
$\nu_7^{C_2H_3F}$	1148.9	1132.5	−16.4
$\nu_8^{C_2H_3F}$	925.0	914.0	−11.0
$\nu_{11}^{C_2H_3F}$	861.6	870.9	+9.3
$\nu_{12}^{C_2H_3F}$	711.8	708.5	−3.3

[a] Not infrared active: using the observed frequencies for $\nu_1^{BF_3} + \nu_4^{BF_3}$ and $\nu_4^{BF_3}$, the $\nu_1^{BF_3}$ frequency is expected to appear near 884 cm^{-1}.

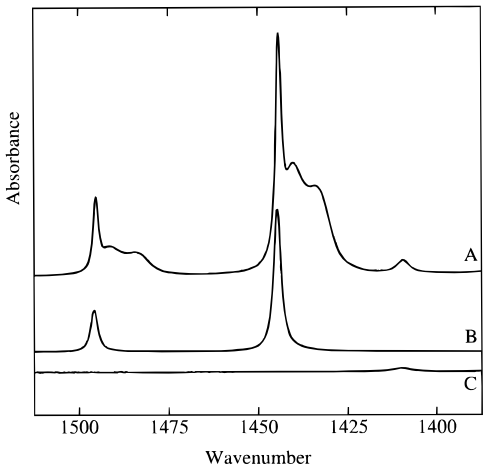

Figure 3. The $\nu_3^{BF_3}$ region of a C_2H_3F/BF_3 mixture dissolved in (A) liquefied argon, of a (B) solution containing only BF_3, and of a (C) solution containing only C_2H_3F. For all spectra, the temperature of the solution was 88 K.

Upon annealing the matrix to 15 K, the intensity of the 1153.3 and the 957.5 cm^{-1} bands rapidly decreases, while that of the bands at 1126.7, 911.6, and 872.9 cm^{-1} slightly increases. Thus,

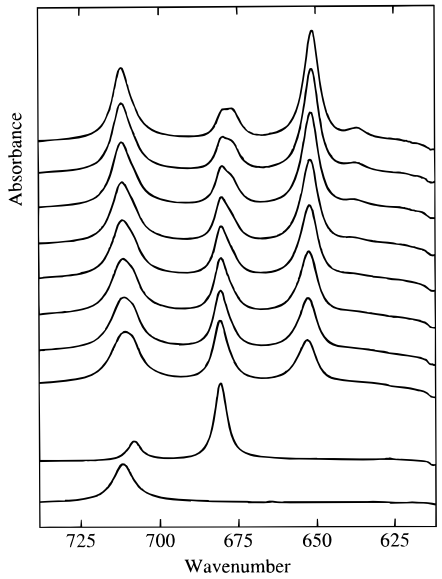

Figure 4. The $\nu_2^{BF_3}$ region of a C_2H_3F/BF_3 mixture dissolved in liquefied argon. The lower two spectra were recorded from solutions containing only BF_3 and C_2H_3F, respectively. For the other spectra, the temperature of the solutions increases from top to bottom, from 88 to 105 K.

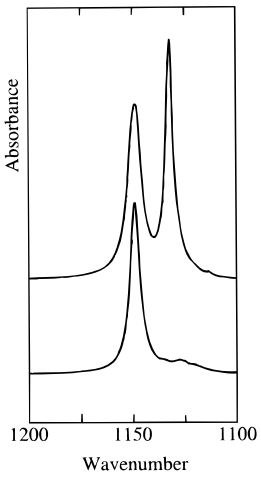

Figure 5. The 1200−1100 cm^{-1} region of a C_2H_3F/BF_3 mixture dissolved in liquefied argon (top) and of a solution containing only C_2H_3F (bottom). For all spectra, the temperature of the solution was 114 K.

even at the relatively low annealing temperatures used, the π complex is converted into the σ complex. This demonstratess that the π complex is less stable than the σ complex which, of course, agrees with the stabilities predicted by ab initio, and with the conclusions drawn from the cryosolution spectra.

For σ-$C_2H_3F \cdot BF_3$ a red shift of 7.1 cm^{-1} was predicted for the $\nu_{10}^{C_2H_3F}$ complex band, but no such band was observed in the spectra of the cryosolutions. It is clear from Figure 8, however, that when doping the C_2H_3F/Ar matrix with BF_3, the intensity ratio of the 929.3/922.0 cm^{-1} bands is remarkably changed. This suggests that close to the monomer $\nu_8^{C_2H_3F}$ band, a complex band must be present. This band is assigned as $\nu_{10}^{C_2H_3F}$ in the σ complex. The observations are compatible with a complexation shift of approximately −6 cm^{-1}, in neat agreement with the ab initio predictions.

2. Stoichiometry of the Observed Species

To establish the stoichiometry of the major complex observed in the cryosolutions, an analysis of the intensities in a concentra-

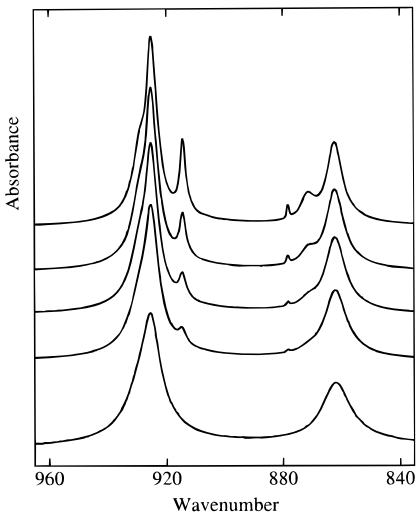

Figure 6. The 960−840 cm^{-1} region of a C_2H_3F/BF_3 mixture dissolved in liquefied argon. The bottom spectrum was recorded from a solution containing only vinyl fluoride. For the other spectra, the temperature of the solution increases from top to bottom, from 88 to 99 K.

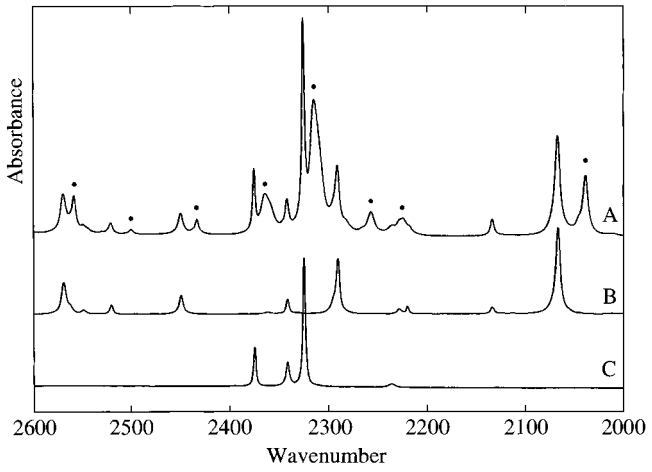

Figure 7. The 2600−2000 cm^{-1} region of a C_2H_3F/BF_3 mixture dissolved in (A) liquefied argon, of a (B) solution containing only C_2H_3F, and of a (C) solution containing only BF_3. For all spectra, the temperature of the solution was 104 K. The bands due to σ-$C_2H_3F{\cdot}BF_3$ are marked with "•".

TABLE 6: Observed Vibrational Frequencies (cm^{-1}) for the σ- and π-$C_2H_3F{\cdot}BF_3$ Complexes Appearing in Solid Argon Matrixes (8 K)

			$C_2H_3F{\cdot}BF_3$ σ complex		$C_2H_3F{\cdot}BF_3$ π complex	
		C_2H_3F (ν)	ν	$\Delta\nu$	ν	$\Delta\nu$
$\nu_7^{C_2H_3F}$	C−F stretch	1148.4	1126.7	−21.7	1153.3	+4.9
$\nu_{10}^{C_2H_3F}$	C═C−H out of plane	929.3	923	−6	957.5	+28.2
$\nu_8^{C_2H_3F}$	CH_2 rocking	923.4	911.6	−11.8		
$\nu_{11}^{C_2H_3F}$	CH_2 wagging	863.2	872.9	+9.7		

tion series was initiated. In this analysis, the intensity of a complex band I_c is plotted, for various integer values of x and y, against $(I_{C_2H_3F})^x(I_{BF_3})^y$, where $I_{C_2H_3F}$ and I_{BF_3} are monomer band intensities.[3,15] For the present case, infrared spectra of solutions containing different concentrations of vinyl fluoride, varying from 5.0×10^{-4} to 1.0×10^{-2} mol L^{-1}, and of BF_3, varying from 1.0×10^{-4} to 1.0×10^{-3} mol L^{-1}, were recorded at a constant temperature of 98.7(3) K. For monomer BF_3 and for the complex the intensities were obtained from a least-squares

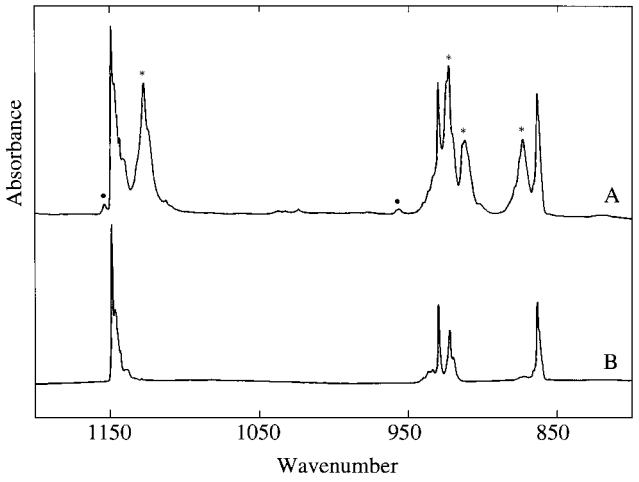

Figure 8. The 1200−800 cm^{-1} region of (A) a C_2H_3F/BF_3 mixture deposited in solid argon and (B) a matrix containing only vinyl fluoride. The concentration ratios for (A) and (B) are 1:1:500 and 1:500, respectively. For both spectra, the temperature of the matrix was 8 K. The bands due to σ-$C_2H_3F{\cdot}BF_3$ and π-$C_2H_3F{\cdot}BF_3$ are marked with "*" and "•", respectively.

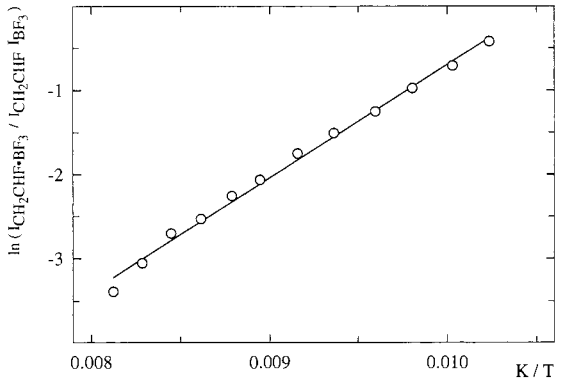

Figure 9. van't Hoff plot for σ-$C_2H_3F{\cdot}BF_3$ dissolved in liquid argon.

band fitting of the $\nu_1^{BF_3} + \nu_3^{BF_3}$ region, while for $I_{C_2H_3F}$ the intensity of $2\nu_{C-F}$ at 2257 cm^{-1} was used. With these intensities, plots were prepared using 1 and 2 as values for x and y. Linear regression on these plots leads to χ^2 values equal to 0.4 (1:1), 186.4 (2:1), 74.4 (1:2), and 120.3 (2:2). The smallest value occurring for $x = y = 1$ proves that, as anticipated above, the major complex has a 1:1 stoichiometry.

The weakness of the bands assigned to the 1:2 complex, and their overlap with bands due to the 1:1 complex prevented the confirmation of the stoichiometry of this second complex by the same techniques.

3. Complexation Enthalpy of the σ Isomer

The complexation enthalpy $\Delta H°$ for σ-$C_2H_3F{\cdot}BF_3$ was derived from a van't Hoff plot. The latter was constructed by plotting the logarithm of the intensity ratio $I_c/[I_{C_2H_3F}I_{BF_3}]$, measured at different temperatures, versus $1/T$. The slope of the plot, corrected for thermal expansion of the solution,[16] equals $\Delta H°/R$. For the present study, solutions containing approximately 5.0×10^{-3} M C_2H_3F and 1.0×10^{-3} M BF_3 were recorded at 12 different temperatures between 97 and 123 K. The resulting van't Hoff plot, obtained using the integrated intensities of the same monomer and complex bands as in the concentration study described above, is shown in Figure 9. From the slope of the linear regression line, corrected for the density variation of the solution,[16] the complexation enthalpy $\Delta H°_{LAr}$ was calculated to be −11.2(3) kJ mol^{-1}.

Discussion

The complexation enthalpy obtained in LAr does not measure the stability of the isolated complex, because of solvent influences.[13,17] The latter, for the monomers and for the complexes, were estimated from ab initio reaction field calculations, using a procedure outlined before.[3,13] In a first step, the liquid phase ΔH°_{LAr} is transformed into a gas phase complexation enthalpy ΔH°_{gas} by applying solvation corrections obtained from SCRF/SCIPCM calculations.[18] In the second step, straightforward statistical thermodynamics[19] is applied to transform the gas phase ΔH° into a complexation energy, so that comparisons can be made with the ab initio results. The solvation energies were calculated at the RHF/6-31+G(d) level and were found to be 2.43, 3.88, and 4.25 kJ mol^{-1} for C_2H_3F, BF_3, and σ-$C_2H_3F{\cdot}BF_3$, respectively. Equating, as before,[3,13] these energies to solvent enthalpies, it follows that in liquid argon the σ complex is less stable by 2.06 kJ mol^{-1} than in the gas phase. Using this value, and using the experimental ΔH°_{LAr} of $-11.2(3)$ kJ mol^{-1}, ΔH°_{gas} is calculated to be $-13.3(3)$ kJ mol^{-1}. The translational and rotational thermal corrections to ΔH°_{gas} were calculated in the classical limit, and the vibrational thermal and zero point energies were calculated using the harmonic ab initio frequencies. The resultant gas phase complexation energy ΔE_{gas} was found to be $-15.2(3)$ kJ mol^{-1}.

It is clear that for the σ complex, the gas phase complexation energy as determined above agrees better with the uncorrected ab initio complexation energy $\Delta E_{ab\ initio}$ than with the BSSE-corrected value $\Delta E^{corr}_{ab\ initio}$. The poor agreement for the BSSE corrected values has been noted previously and was attributed to the counterbalancing effect of the basis set incompletness error (BSIE) when a small basis set such as 6-31+G(d) is used.[3,20,21] As BSIE is not accounted for during the counterpoise correction, the results obtained above again confirm that for a comparison with experiment the uncorrected complexation energy $\Delta E_{ab\ initio}$ must be preferred.

As discussed above, in the spectra of the matrixes also weak bands due to a less stable π complex were observed. As the solid matrixes were obtained by condensing a room temperature gas mixture, this suggests that in addition to the σ complex, also a measurable fraction of π complex must be formed at room temperature. Using the spectra shown in Figure 9, and using the calculated infrared intensities given in Tables 3 and 4, the approximate concentration ratio [σ-$C_2H_3F{\cdot}BF_3$]/[π-$C_2H_3F{\cdot}BF_3$] calculated from the freshly deposited matrix was close to 15. From this, assuming that during deposition of the matrix the room-temperature equilibrium was frozen out, the concentration of the π complex at room temperature can be estimated to be close to 6% of that of the σ complex.

The relative populations of σ and π complexes in the vapor phase can also be obtained by converting the ab initio complexation energy into a standard free enthalpy difference ΔG° using statistical thermodynamics. As above, the ab initio frequencies and rotational constants were used, and the calculations were made at 300 K and at 100 K, the latter being a typical temperature used for the cryosolutions. The results are summarized in Table 7.

It can be seen in Table 7 that at 300 K the free enthalpy difference $\Delta G^\circ = \Delta H^\circ - T\Delta S^\circ$ between the σ and the π complex equals -6.03 kJ mol^{-1} for the uncorrected complexation energies and -4.46 kJ mol^{-1} for the BSSE corrected values. Using $\Delta G^\circ = -RT \ln K$ the σ to π concentration ratios were calculated to be 11.2 (8% π-$C_2H_3F{\cdot}BF_3$) and 6 (14% π-$C_2H_3F{\cdot}BF_3$), respectively. The former value is close to the value of 6% derived from the matrix experiment, while the value obtained from the corrected interaction energies is overestimated. This appears to support the above conclusion that the uncorrected value for the interaction energy is closer to the real value. The excellent agreement, however, may be somewhat fortuitous. As noted above, the π complex is completely converted into the more stable σ complex by annealing at a mere 15 K. This shows that the activation energy for the conversion is very low. Therefore, it is not impossible that during the deposition of the matrix at 8K some of the π complex already is converted, i.e., the vapor phase equilibrium population derived from the matrix spectra maybe is slightly too low.

TABLE 7: Energy Difference and Standard Enthalpy, Entropy, and Free Enthalpy Differences between σ-$C_2H_3F{\cdot}BF_3$ and π-$C_2H_3F{\cdot}BF_3$ at 100 and 300 K

	300 K		100 K		
	model 1[a]	model 2[b]	model 1[a]	model 2[b]	units
$\Delta E = E_\sigma - E_\pi$	−6.82	−5.25	−6.82	−5.25	kJ mol^{-1}
$\Delta H^\circ = H_\sigma - H_\pi$	−7.23	−5.65	−7.20	−5.63	kJ mol^{-1}
$\Delta S^\circ = S_\sigma - S_\pi$	−3.999	−3.999	−4.739	−4.739	J mol^{-1} K^{-1}
$\Delta G^\circ = \Delta H^\circ - T\Delta S^\circ$	−6.03	−4.45	−6.73	−5.16	kJ mol^{-1}
% σ-$C_2H_3F{\cdot}BF_3$	91.8	85.7	99.97	99.80	
% π-$C_2H_3F{\cdot}BF_3$	8.2	14.3	0.03	0.20	

[a] Based upon the MP2/6-31+G(d) interaction energies before BSSE correction. [b] Based upon the MP2/6-31+G(d) interaction energies after BSSE correction.

Using a similar analysis, and using the uncorrected complexation energies for the complexes, the vapor phase ΔG° between σ and π complex at 100 K was calculated to be -6.73 kJ mol^{-1}. For a comparison with the experimental data deduced from the cryosolutions, this value needs to be corrected for the solvent influences. Therefore, also for π-$C_2H_3F{\cdot}BF_3$ the solvation energy was calculated by using the SCRF/SCIPCM model described above. From the resulting values for σ and π complex, the free energy difference ΔG° for a solution in liquid argon was then estimated to be -6.22 kJ mol^{-1}. From this, the σ to π concentration ratio in a LAr solution at 100 K was derived to be 1.8×10^3. This ratio bears out our conclusion that the concentration of the π complex in our cryosolutions was below the detection limit.

Some time ago, Legon and Millen proposed[22,23] three rules with which the angular geometry of hydrogen bonded complexes B···HX, where X is a halogen or a pseudohalogen, can be predicted. According to these rules, the electrophilic end δ^+H of HX seeks the direction of the greatest nucleophilicity in the Lewis base. The rules also state that Lewis bases in which free electron pairs and π bonds are simultaneously present, the interaction with the nonbonding electron pair is the stronger one. In a recent paper,[24] the rules were extended to include the complexes formed with chlorine monofluoride, ClF. It was found that the angular geometry is almost completely determined by the electrostatic interaction between the electrophilic end δ^+Cl of ClF and a nonbonding electron pair or π-bonding electron pair of the Lewis base.

In the present case, the Lewis acid is BF_3. The atomic charge on the boron atom has been estimated to be $+1.5e$,[3,25] and from this it is obvious that the boron atom is the electrophilic center. The observation in this study that with vinyl fluoride, which contains both a π bond and free electron pairs, the σ complex is formed suggests that the Legon−Millen rules[22−24] can be used to make predictions on BF_3 complexes as well.

Acknowledgment. W.A. Herrebout is indebted to the Fund for Scientific Research (FWO, Belgium) for an appointment as Postdoctoral Fellow. The FWO is also thanked for financial help

toward the spectroscopic equipment used in this study. Financial support by the Flemish Community, through the Special Research Fund (BOF), is gratefully acknowledged. The authors thank the CSC, Center for Scientific Computing Ltd. (Espoo, Finland), for generously providing the computer mainframe time and facilities.

References and Notes

(1) Sluyts, E. J.; Van der Veken, B. J. *J. Phys. Chem.* **1997**, *101A*, 9070.
(2) Sluyts, E. J. Ph.D. Thesis, University of Antwerp, Antwerp, **1997**, p 274.
(3) Herrebout, W. A.; Van der Veken, B. J. *J. Am. Chem. Soc.* **1997**, *119*, 10446.
(4) Kisiel, Z.; Fowler, P. W.; Legon, A. C. *J. Chem. Phys.* **1990**, *93*, 3054.
(5) Herrebout, W. A.; Van der Veken, B. J. *J. Chem. Soc., Faraday Trans.* **1997**, *93*, 3453.
(6) Frisch, M. J.; Trucks, G. W.; Schlegel, H. B.; Gill, P. M. W.; Johnson, B. G.; Robb, M. A.; Cheeseman, J. R.; Keith, T.; Petersson, G. A.; Montgomery, J. A.; Raghavachari, K.; Al-Laham, M. A.; Zakrzewski, V. G.; Ortiz, J. V.; Foresman, J. B.; Cioslowski, J.; Stefanov, B. B.; Nanayakkara, A.; Challacombe, M.; Peng, C. Y.; Ayala, P. Y.; Chen, W.; Wong, M. W.; Andres, J. L.; Replogle, E. S.; Gomperts, R.; Martin, R. L.; Fox, D. J.; Binkley, J. S.; Defrees, D. J.; Baker, J.; Stewart, J. P.; Head-Gordon, M.; Gonzalez, C.; Pople, J. A. *Gaussian 94*, Revision E2; Gaussian, Inc.: Pittsburgh, PA, 1995.
(7) Peng, C.; Ayala, P. Y.; Schlegel, H. B.; Frisch, M. J. *J. Comput. Chem.* **1996**, *17*, 49.
(8) Boys, S. B.; Bernardi, F. *Mol. Phys.* **1970**, *19*, 553.
(9) Gutman, V. *The Donor Acceptor Approach to Molecular Interactions*; Plenum Press: New York, 1988.
(10) Stolov, A. A.; Herrebout, W. A.; Van der Veken, B. J. *J. Am. Chem. Soc.* **1998**, *120*, 7310.
(11) Smith, G. R.; Guillory, W. A. *J. Chem. Phys.* **1975**, *63*, 1311 and references cited therein.
(12) Sluyts, E. J.; Van der Veken, B. J. *J. Am. Chem. Soc.* **1996**, *118*, 440.
(13) Herrebout, W. A.; Everaert, G. P.; Van der Veken, B. J.; Bulanin, M. O. *J. Chem. Phys.* **1997**, *107*, 8886.
(14) Herrebout, W. A.; Van der Veken, B. J. *J. Am. Chem. Soc.* **1998**, *120*, 9921.
(15) Van der Veken, B. J. In *Low-Temperature Molecular Spectroscopy*; Fausto, R., Ed.; Kluwer Academic: Dordrecht, 1996.
(16) Van der Veken, B. J. *J. Phys. Chem.* **1996**, *100*, 17436.
(17) Herrebout, W. A.; Van der Veken, B. J. *J. Phys. Chem.* **1996**, *100*, 9671.
(18) Foresman, J. B.; Keith, T. A.; Wiberg, K. B.; Frisch, M. J. *J. Phys. Chem.* **1996**, *100*, 16098.
(19) Scheiner, S. *Hydrogen Bonding: a Theoretical Perspective*; Oxford University Press: Oxford, 1997; p 15.
(20) Everaert, G. P.; Herrebout, W. A.; Van der Veken, B. J.; Lundell, J.; Räsänen, M. *Chem. Eur. J.* **1998**, *4*, 321.
(21) Jonas, V.; Frenking, G.; Reetz, M. T. *J. Am. Chem. Soc.* **1994**, *116*, 7714.
(22) Legon, A. C.; Millen, D. J. *Faraday Discuss. Chem. Soc.* **1982**, *73*, 77.
(23) Legon, A. C.; Millen, D. J. *Chem. Soc. Rev.* **1986**, *16*, 467.
(24) Legon, A. C. *Chem. Phys. Lett.* **1997**, *297*, 55.
(25) Fowler, P. W.; Stone, A. J. *J. Phys. Chem.* **1987**, *91*, 509.